DJS Vol. 49(2)(2024) – pp. 82-98 ISSN: 1012-5965

Delta Journal of Science
Available online
at https://djs.journals.ekb.eg/

Research Article

CHEMISTRY

Encapsulation of organomontmorillonite platelets through miniemulsion polymerization inside poly(methyl methacrylate) latex particles: synthesis and thermal properties

Ahmed Akelah, Ahmed Rehab, Hisham Harhash, Hamada S. A. Mandour*

Polymer Research Group, Chemistry Department, Faculty of Science, Tanta University, Tanta 31527, Egypt

***Corresponding author**: Dr. Hamada Mandour **e-mail**: hamada.mandour@science.tanta.edu.eg

Received: 6/12/2024 **Accepted:** 2 /1/2025

KEY WORDS

Montmorillonite, Poly(Methyl methacrylate), Miniemulsion, Nanocomposite, Encapsulation

ABSTRACT

In this study, encapsulation of montmorillonite (MMT) platelets into poly(methyl methacrylate) (PMMA) was successfully achieved via miniemulsion polymerization. First, *N*-allyl-*N*,*N*-dimethyloctadecan-1-aminium bromide (ADM_{18}), a polymerizable surfactant, was employed to modify MMT nanoplatelets via ion exchange to improve the compatibility with the matrix phase as well as form a covalent anchor with PMMA. Subsequently, MMT-ADM_{18} was incorporated in methyl methacrylate, along with a surfactant, costabilizer, and initiator, to obtain stable nanocomposite latexes via miniemulsion polymerization. FTIR (Fourier transform infrared spectroscopy), XRD (X-ray diffraction), SEM (Scanning electron microscopy), TEM (Transmission electron microscopy), and TGA (Thermogravimetric analysis) were utilized to validate structures and characterize thermal properties of neat PMMA and PMMA-based nanocomposites. FTIR indicated an interaction occurred between MMT's structural OH groups and PMMA's carbonyl moiety. XRD exhibited that the nanocomposites' morphology exfoliated. TEM images demonstrated stable nanocomposite latexes comprised of MMT core and PMMA shell with diameters ranging from 320 to 450 nm were formed. The TGA results showed a substantial improvement in nanocomposites' thermal stability, as evidenced by shifting the onset of the thermal degradation compared to that for pristine PMMA.

Introduction

Layered silicate-based polymeric nanocomposites have received immense academic and industrial attention because of their exceptional attributes and diverse applications **(Kalendova *et al.*, 2024; Murugesan *et al.*, 2020; Guo *et al.*, 2018)**. Layered silicates possess exquisite thermal, mechanical, fire, and barrier properties, and the intent is to imbue polymeric materials with these properties even at very small loading (about 5%) to produce nanocomposite materials that satisfy requirements for advanced applications **(Abulyazied *et al.*, 2021; Bee *et al.*, 2018)**. The exfoliation of the silicate layers resulting from the uniform dispersion of ultrafine silicate platelets inside the polymer matrix is the primary feature causing much-improved performance **(Abuzeid *et al.*, 2024; Dastjerdi *et al.*, 2019; Yu *et al.*, 2018)**. Phyllosilicate clays of the 2:1 type, and especially montmorillonite (MMT), are frequently employed as inorganic reinforcing materials among a wide variety of materials used to produce nanocomposites **(Idumah *et al.*, 2022)**. MMT is a layered hydrated aluminum phyllosilicate that exhibits a platy morphology consisting of two sheets of silicate/aluminum oxide with a corner-linked tetrahedra structure and an edge-shared octahedral sheet sandwiched in between **(Gul *et al.*, 2016)**. The dispersion status of clay platelets throughout the polymeric matrix is a significant consideration to take into account while preparing layered silicate nanocomposites. Most hydrophobic polymers are incompatible with pristine clay nanoparticles, and platelet stacking is frequently observed, making it difficult to obtain the desired final nanocomposite features. Because of the inherent hydrophilic properties and high surface energy, organic modification is an inevitable step towards rendering clay's hydrophilic surface more hydrophobic. An often-used strategy is the ion exchange reaction between organic cations (typically amines or phosphates attached to long aliphatic chains) and positive inorganic cations. The basal-plane spacing widening and gallery hydrophilicity loss are brought about by organic modification; more monomers were able to enter the interlayer, causing intercalation and exfoliation. The degree of interphase strength between the silicate and the polymeric matrix determines whether a polymeric nanocomposite based on layered silicate is intercalated or exfoliated **(Franco-Urquiza, 2021; Guo *et al.*, 2020; Zhu *et al.*, 2019; Uddin, 2018)**. Several elaboration approaches have been considered where either the nanocomposite is created from the polymer or directly from the monomer. These methods include in-situ polymerization, solution casting, and melt-intercalating. Because there are so many distinct polymerization conditions and clay treatments that can be employed for obtaining exfoliated morphology and

dispersion matrix-compatible character, in-situ polymerization is the approach of choice **(Uddin *et al.*, 2024; Okamoto, 2023)**. Water-borne polymerization is becoming more prevalent among various in-situ polymerization routes than conventional solvent-borne technologies because it is easier to implement and more environmentally friendly (because it relies on water as a continuous phase) when making polymer-clay nanocomposites. Of all the water-borne polymerization processes that exist, aqueous emulsion-based polymerization is the most efficient approach for synthesizing water-borne polymeric nanocomposites. Conventional emulsion polymerization is the most frequently used technique to produce latexes **(Dastjerdi *et al.*, 2019; Yu *et al.*, 2018)**. Emulsion polymerization is a heterogeneous free radical polymerization that spreads the monomer into droplets roughly 10 µm in diameter. The surfactant's adsorption at the monomer-water interface is liable for droplet stability. In emulsion polymerization, monomers diffuse and transfer from macrodroplets to monomer-swollen micelles, causing particle growth **(Lovell *et al.*, 2020)**. There are drawbacks to this process, such as a lack of particle size uniformity; thus, miniemulsion polymerization is highlighted for the production of colloidal nanocomposites owing to the 1-to-1 mechanism, which means the polymer particles are replicas of the miniemulsion droplets **(Schork, 2024)**. Combining high shear, which breaks the emulsion into submicron monomer droplets, and an appropriate costabilizer/surfactant system that prevents droplet collisions and diffusional degradation, produces miniemulsion. The polymerization is carried out by radical entrance into the preexisting miniemulsion droplets, each of those droplets may be thought of as an individual nanoreactor **(Álvarez-Bermúdez *et al.*, 2024; Pieters *et al.*, 2024; Jansen *et al.*, 2016)**. Miniemulsion polymerization has shown effectiveness in encapsulating a variety of inorganic particles, the majority of which are spherical **(Thickett *et al.*, 2019; Muñoz-Espí *et al.*, 2012)**. However, encasing high-aspect ratio inorganic particles presents further challenges due to their ability to form stacks and card-house structures **(Faucheu *et al.*, 2010; Zengeni *et al.*, 2013)**. Only a few studies have attempted to encapsulate MMT platelets inside latex particles via miniemulsion polymerization **(Voorn *et al.*, 2006; Silva *et al.*, 2019)**. The high viscosity of the organic phase has mainly restricted the percentage of encapsulated clay to 4%.

Consequently, the MMT cannot be finely distributed, which will eventually lead to colloidal instability **(Zengeni *et al.*, 2013)**. One of the most prevalent optical matrix polymer to produce transparent polymer nanocomposites is poly(methyl methacrylate) (PMMA). PMMA has several outstanding properties, such as non-toxicity, dimensional stability, and impact strength. PMMA is, however, lacking in

heat resistance or thermal stability, therefore, while retaining optical clarity, PMMA-MMT nanocomposites offer the potential for reduced gas permeability, enhanced physical performance, and improved heat resistance **(Akelah *et al.*, 2017; Zidan, 2020)**. This work focuses on synthesizing and characterizing PMMA-encapsulated nanoscale MMT platelet nanocomposites generated through the miniemulsion polymerization technique. MMT was modified using polymerizable cationic surfactant and then copolymerized with MMA monomer, causing exfoliation and facilitating encapsulation. The new nanocomposites will be characterized by morphological and thermal characterization.

Experimental

Materials

Sodium montmorillonite (Na-MMT) was supplied from ECC America Inc. with a cation exchange capacity of 0.9 mequiv/g. *N*-allyl-*N*,*N*-dimethyl-stearyl ammonium bromide (ADM_{18}) was synthesized and characterized by ^{1}H NMR and mass spectroscopy according to the previous study **(Mang *et al.*, 2010; Bai *et al.*, 2020)**. Methyl methacrylate (MMA, Sigma-Aldrich) was freed from phenolic inhibitors by shaking with 5% NaOH solution followed by washing with water and drying over anhydrous Na_2SO_4. Hexadecane (HD, BDH Chemicals Ltd.), sodium dodecyl sulphate (SDS, Techno Pharma), potassium peroxodisulphate (KPS, Fisher Scientific), and sodium hydrogen carbonate were used as received.

Instruments

Fourier transform infrared spectroscopy (FTIR) spectra were recorded using a JASCO FTIR-4100 spectrometer (Japan). The spectra were acquired utilizing the KBr pressed disk technique over a spectral range of 4000-400 cm^{-1}.

X-ray diffraction (XRD) measurements were conducted on a Phillips PW1710 instrument with a Cu-Ka radiation source (λ =0.154 nm) at room temperature. Diffraction intensities were recorded in the (2θ) range of 3°-80° with a step width of 0.02°.

Thermogravimetric analysis (TGA) was performed on a Shimadzu thermogravimetric instrument (TGA 50 series). Under nitrogen protection, the samples were heated at a rate of 10 °C/min from 30 to 800 °C.

Scanning electron microscopy (SEM) and transmission electron microscopy (TEM) were used to study the nanomorphology of PMMA/MMT-ADM_{18} nanocomposites. SEM images were taken on a JEOL JSM-IT200 operated at a 20 kV accelerating voltage. SEM with a detector for energy-dispersive X-ray (EDX). TEM images were captured utilizing a JEOL JEM-1400 Plus with a 120 kV accelerating voltage. The sample was prepared by evaporating drops of a PMMA/MMT-ADM_{18} nanocomposite-ethanol suspension after sonication onto a copper grid.

Methods

Modification of MMT by ADM_{18}

The cation-exchange reaction was performed by swelling 3 g of MMT overnight in 90 mL of distilled water. Then, 10 mL of dioxane was added, and stirring was continued for 2 h. To the stirred-hot (60°C) clay suspension, a solution containing 1.64 g of ADM_{18} in 30 mL of dioxane was continuously added dropwise under vigorous stirring for 2 h. The cationic exchange was carried out at 60°C for 5 h. Afterward, the MMT-ADM_{18} was filtrated and washed repeatedly with hot 90:10 water/dioxane (v/v) in order to get rid of excess ADM_{18} molecules, and then dried in a vacuum oven at room temperature **(Agag *et al.*, 2008; Agag *et al.*, 2010)**.

Incorporating MMT-ADM_{18} into PMMA latex via miniemulsion polymerization

The recipe used for encapsulating MMT-ADM_{18} in PMMA latex is tabulated in Table (1). SDS (0.13 g) was dissolved in 30 mL water and then stirred for 60 min. The oil phase comprising MMT-ADM_{18} (0.05 g) swelled in MMA (5 g) and HD (0.2 g) was magnetically stirred overnight after being ultrasonically stirred for 10 min in an ice bath. The oil phase was then added to the aqueous phase, and the mixture was left to stir for 60 min at 1500 rpm under ice cooling for pre-emulsification. Then, the mixture was homogenized by using rotor-stator homogenization in an ice bath for 10 min to prevent self-polymerization. The miniemulsion was transferred to a 100 ml three-neck round-bottom flask containing $NaHCO_3$ solution (10 mM), equipped with a condenser and a mechanical stirrer. Once the system reached the ambient temperature of 80°C, the KPS solution (0.12 g in 10 g of water) was added over 10 min. The polymerization was maintained for 24 h after injecting the initiator solution. After being cooled, the emulsion was added to MeOH for coagulation, then washed with water and dried in a vacuum oven at 30°C. For comparison, neat latex and PMMA/MMT-ADM_{18} nanocomposite containing 3% MMT-ADM_{18} were prepared by the same method. The monomer conversion was up to 95%.

Table (1): Summary of the composition of the continuous phase and dispersed phase used to prepare the PMMA/MMT-ADM_{18} nanocomposite.

	Components	Weight (g)
Monomer phase	MMA	5.0
	MMT-ADM_{18}	0.05-0.1
	HD	0.2
Aqueous phase	Water	45.0
	SDS	0.13
	KPS	0.12
	$NaHCO_3$	0.04

Results and discussion

Characterization of MMT-ADM$_{18}$

To improve MMT wettability with the polymer phase and facilitate encapsulation into monomer droplets upon emulsification, *N*-allyl-*N*,*N*-dimethyl-stearyl ammonium bromide (ADM$_{18}$) was selected to be exchanged with the sodium ions present in the interlayer space of MMT. The cation exchange reaction was characterized by XRD, FTIR, and TGA analyses, as previously described. XRD analysis is used to study the gallery structure of the silicate. XRD traces are presented in Fig. (1). The characteristic diffraction peak of MMT at around 7.18° (2θ) was displaced to a lower angle (4°) after organic modification. The interlayer distance was enlarged from 1.22 nm to 2.18 nm at a large extent of cation exchange. This result evidenced an increase in interlamellar space due to larger ADM$_{18}$ ions successfully replacing smaller Na^+ ions located in MMT lamellar galleries **(Agag *et al.*, 2010)**.

The FTIR spectra of MMT and MMT-ADM$_{18}$ are examined in Fig. (2). A characteristic bands of stretching vibrations corresponding to OH oscillations of (Al, Mg) and physically adsorbed H_2O are observed at 3630 and 3448 cm^{-1}. Also, the peak at 1645 cm^{-1} is due to -OH deformation vibration. An intense band corresponding to the stretching vibration of Si–O–Si in layered silicates at 1045 cm^{-1}. The band at 919 cm^{-1} represents Al–Al–OH deformation vibration, as well as Si–O bending vibrations at 523 cm^{-1} **(Yu *et al.*, 2018)**. The spectrum of the MMT-ADM$_{18}$ shows the apparition of new peaks at 2924 and 2852 cm^{-1} attributed to asymmetric and symmetric stretching vibrations of the CH_2 group in the alkyl chain of ADM$_{18}$, as well as the CH_2 bending mode at 1469 cm^{-1}. Simultaneously, the characteristic bands of MMT are also observed in the spectrum of MMT-ADM$_{18}$.

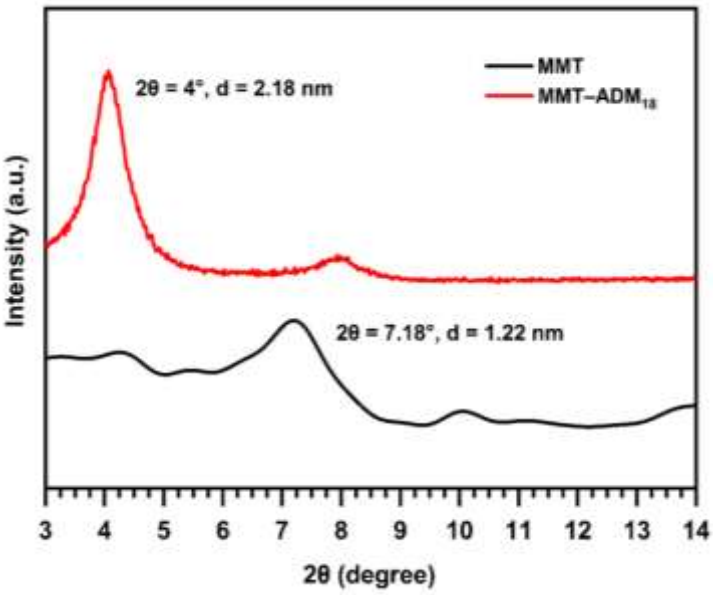

Fig. (1): XRD patterns of MMT and ADM$_{18}$-modified MMT.

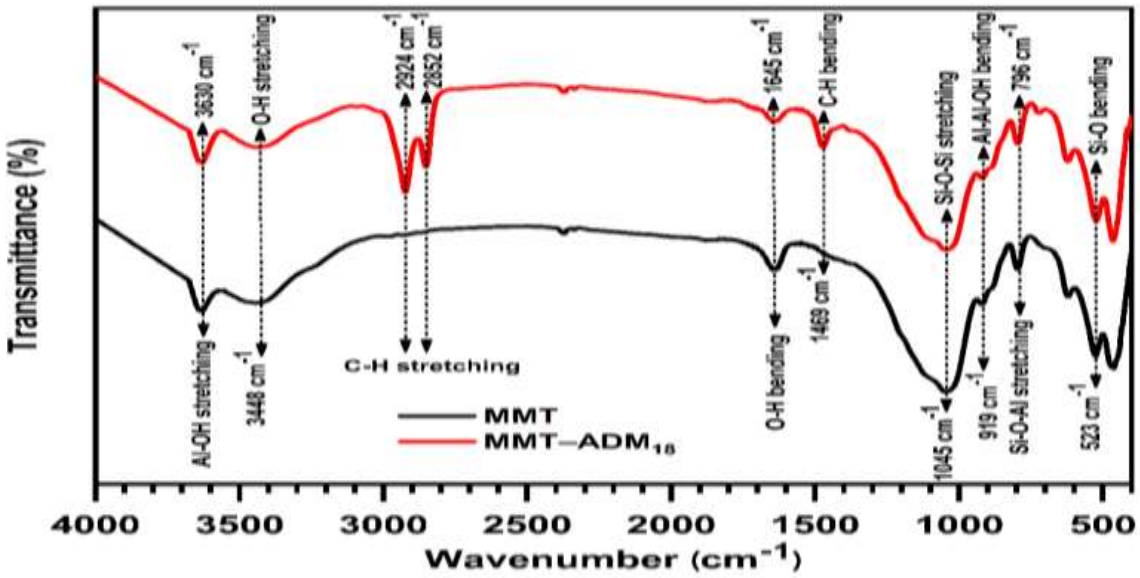

Fig. (2): FTIR spectra of MMT and MMT-ADM_{18}.

The aforementioned results are strongly supported by the obtained TGA results. Figure (3) shows the thermogravimetric degradation profiles of MMT and MMT-ADM_{18}. Below 100°C, about 4% of the physically adsorbed water for MMT is evaporated. After that, the weight of MMT remains almost constant up to 500°C. Then another weight loss of 6.5% for MMT occurred in the range between 500–800°C, corresponding to the dehydroxylation of the layers. Total weight loss of MMT is close to 10.5% **(Chencheni *et al.*, 2024)**. In the decomposition curve of MMT-ADM_{18}, a rapid weight loss starts around 200°C to 350°C due to the degradation of ADM_{18} molecules present outside the clay sheets. Another stage of weight loss appears from 360 to 610°C, which is attributed to the degradation of interlayer ADM_{18} ions, which intercalated through cation exchange **(Moraes *et al.*, 2009)**. Over 610°C, MMT-ADM_{18} continued to lose weight due to dehydroxylation (the structural OH groups). Total weight loss is about 33%. Based on the above-mentioned results, one can say that the ADM_{18} ions successfully intercalated in MMT galleries.

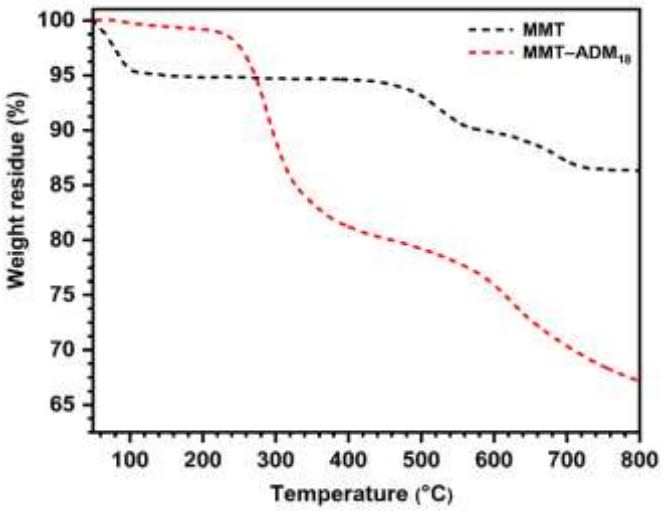

Fig. (3): TGA profiles of MMT and MMT-ADM_{18}.

Miniemulsion polymerization

In contrast to emulsion polymerization, miniemulsion polymerization proceeds via monomer droplet nucleation through converting monomer droplets, which typically have a diameter of 50–500 nm, onto polymer particles. Coalescence and Ostwald ripening can be prevented in miniemulsions by choosing an appropriate surfactant and adding a costabilizer to achieve a consistent droplet size. This technique is a promising route for preparing nanocomposites, usually by encapsulation.

Characterization of colloidal PMMA/MMT-ADM$_{18}$ nanocomposites

FTIR characterization

FTIR was used to prove the inclusion of MMT in the PMAA matrix and to observe if interactions between the components occurred. Figure (4) shows the FTIR spectra of PMMA and PMMA nanocomposites. Spectra of neat PMMA showed methyl, ester-methyl, and methylene C–H stretching vibrations in the region of 3000–2855 cm^{-1}. An intense peak at 1735 cm^{-1} is assigned to C=O stretching vibrations. Peak at 1456 cm^{-1} is ascribed to the C–H bending modes of CH_3 and CH_2 groups. The less–intense band at 1384 cm^{-1} is due to the bending vibration of the C–H bond of the methyl group. The peak located at 1249 cm^{-1} is interpreted as C–C–O stretching vibration. The typical absorption band is observed at 1155 cm^{-1} originating from C–O–C stretching vibration. The peak at 980 cm^{-1} refers to C–O bending mode. The band at 840 cm^{-1} is assigned to the methylene rocking mode, and C–C stretching at 755 cm^{-1} **(Terchi *et al.*, 2024; Youssef *et al.*, 2017)**. As can be seen from the spectra of PMMA/MMT-ADM$_{18}$ nanocomposites, PMMA backbone peaks reappeared again, but the inclusion of MMT-ADM$_{18}$ in the PMMA matrix caused some alteration. The intensity of C=O band decreases and shifts to 1720 cm^{-1} and a new band appeared at 1627 cm^{-1} which attributed to the hydrogen-bonded carbonyl group. The band at 3632 cm^{-1} assigned to stretching vibration of structural OH groups became broad, indicating the interaction between structural OH groups of MMT-ADM$_{18}$ and PMMA. The broad band at 1155 cm^{-1} resulted from coalesced Si–O moieties stretching vibration with C–O–C group vibration.

Also, the intensity of the band at 980 cm^{-1} (C–O bending mode) depressed and coupled with the Al–Al–OH deformation band. Based on these findings, it can be concluded that the MMT not only encapsulated in the PMMA matrix but also interacted with PMAA during polymerization **(Godiya *et al.*, 2021; Al-Sabagh *et al.*, 2016)**.

XRD characterization

XRD was used to study the extent of MMT platelet delamination and the affinity between the polymer chains and MMT. XRD measurements were carried

out for neat PMMA and PMMA nanocomposites with 1 and 3% MMT-ADM_{18} in the 2θ range (3–40°), and diffraction patterns are shown in Fig. (5a). PMMA exhibits two broad peaks at 15° and 30°, confirming the amorphous nature of the PMMA matrix **(Bakr *et al.*, 2024; Al-Muntaser *et al.*, 2020)**. When MMT-ADM_{18} is incorporated into the PMMA matrix, the peak at 15° becomes broader in the nanocomposite spectra, confirming their amorphous structure. In order to examine the morphology of MMT in the nanocomposite, a short scan in the range (3–18°) was performed as illustrated in Fig. 5(b). MMT-ADM_{18} shows a sharp peak at 4° (d-spacing around 2.18 nm). After miniemulsion polymerization and with increasing the MMT-ADM_{18} amount from 1 to 3%, the characteristic peak corresponding to MMT-ADM_{18} vanished in all PMMA/MMT-ADM_{18} nanocomposite spectra, meaning that exfoliated morphology was obtained. This is attributed to the disruption of the orderly nature of MMT platelets. This results from penetrating MMA molecules between the MMT lamellae, expanding the galleries; therefore, more MMA molecules diffuse between layers, exfoliating the MMT.

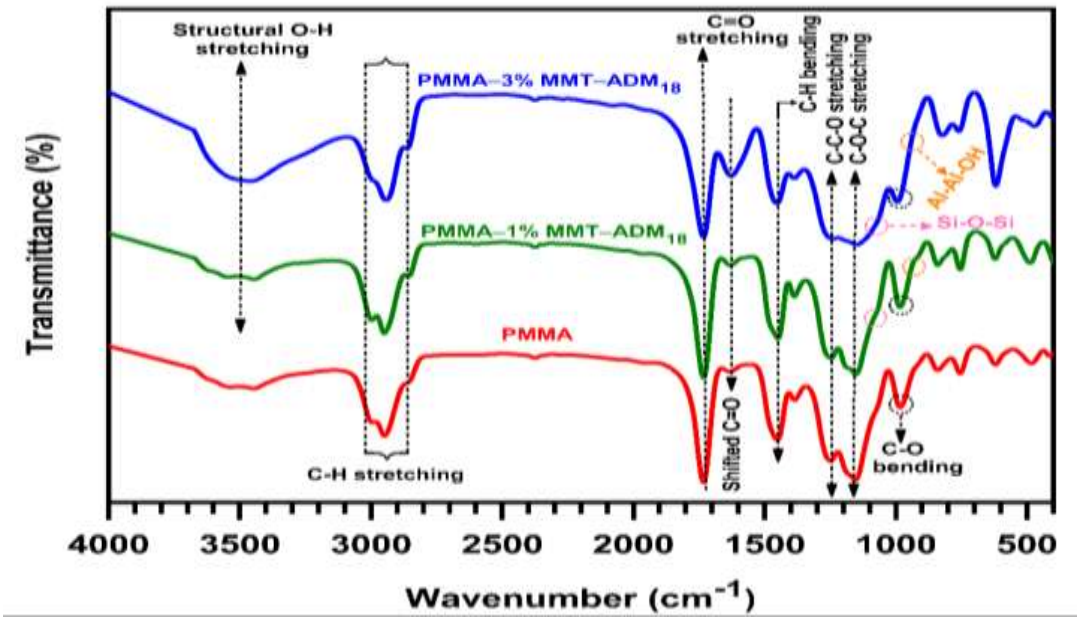

Fig. (4): FTIR spectra of PMMA and PMMA/MMT-ADM_{18} nanocomposites with 1 and 3% MMT-ADM_{18}.

Morphological structure of nanocomposite materials

SEM and TEM were utilized to examine the nanomorphology of PMMA/MMT-ADM_{18} nanocomposites. Figure (6) illustrates TEM photographs of the nanocomposite latex. Figure (6a) displays a TEM image of the latex sample with 1% MMT. The latex's particle size is about 320 nm. As seen from the image, the sample has a dark inner core surrounded by a light, smooth-contoured PMMA shell. The dark domain represents MMT platelets (because of MMT's size, the electron's beam cannot pass across the particles, so it displays as dark). Besides, the latex surface exhibits smooth contours devoid of MMT platelets, indicative of the whole encapsulation of MMT.

After the MMT amount increased to 3%, the particles seemed larger and exhibited a broad size distribution, as shown in Fig. (6b). The particle size became larger (450 nm) compared to that in PMMA (200 nm) **(Wang *et al.*, 2020)**, implying encapsulation of further MMT in the PMMA droplets. The particles maintained their distinctive appearance with a smooth-contoured PMMA shell and an MMT-rich inner core with regular contours.

Figure 7(a) shows a SEM micrograph of the surface of latex particles, which clearly shows a complete and dispersive spherical morphology. The surface of the latex particles is perfectly smooth, which differs from the rugged surface observed for MMT-covered particles **(Cauvin *et al.*, 2005; Voorn *et al.*, 2006)**. Moreover, the elemental composition of the PMMA/MMT-ADM_{18} nanocomposite was examined using EDX combined with SEM Fig. (7b). EDX analysis of the PMMA-3% MMT-ADM_{18} detected a large pinnacle of the **C** element and small pinnacle of **Si** element; these pinnacles are ascribed to the PMMA and MMT structures, respectively. Therefore, it can be inferred from the previous results that the MMT platelets are not located at the surface of the latex not located at the surface of the latex particles but are encapsulated inside the latex particles.

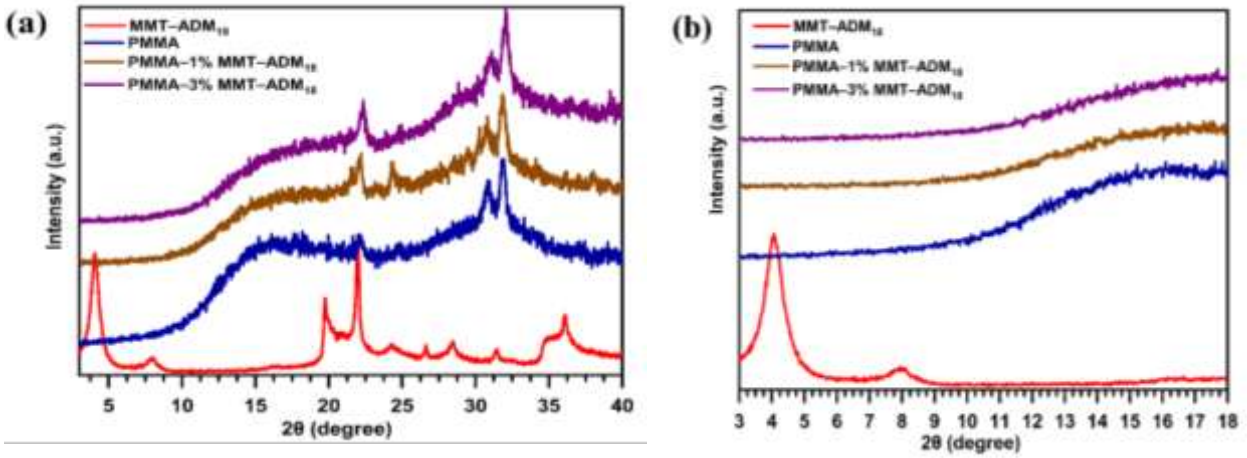

Fig. (5): XRD patterns of PMMA and PMMA/MMT-ADM_{18} nanocomposites with 1 and 3% MMT-ADM_{18}, 2θ ranging from 3 to 40 degrees (a) and from 3 to 18 degrees (b)

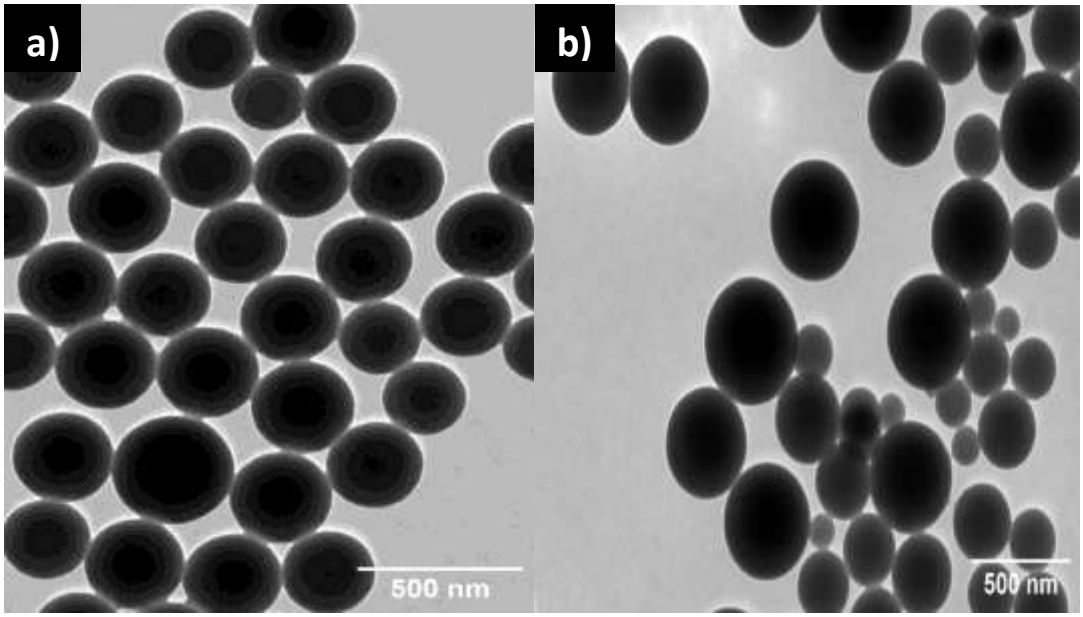

Fig. (6): TEM images of the final latex for samples with (a) 1% MMT-ADM18, (b) 3% MMT-ADM18

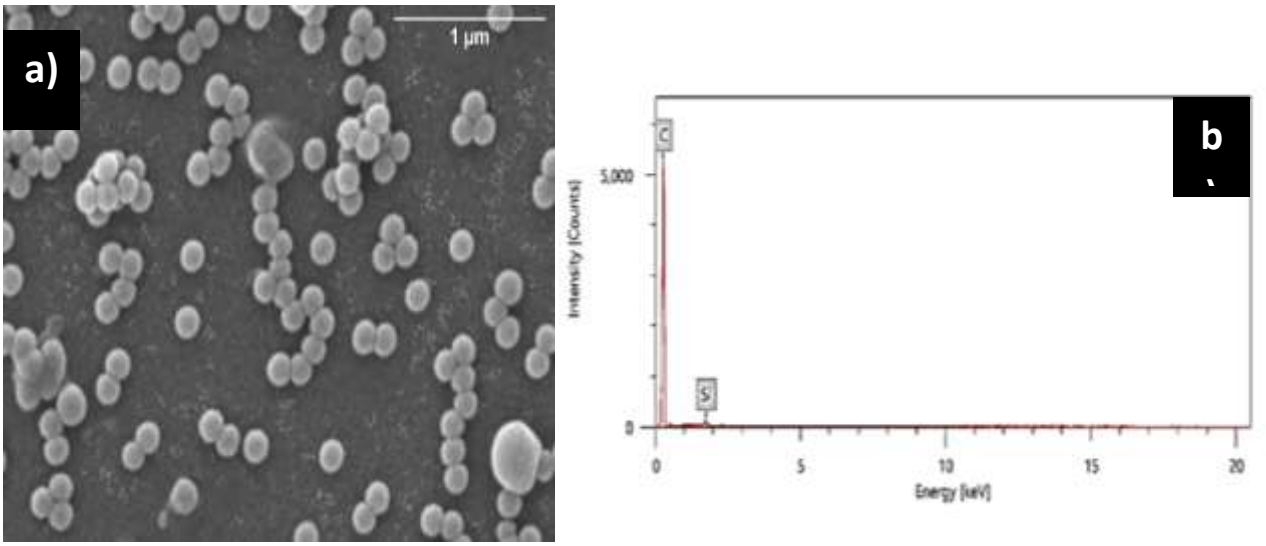

Fig. (7): (a) SEM image of final PMMA nanocomposite latex particles and (b) EDX spectra of the final PMMA nanocomposite latex particles.

Thermal properties

The thermal stability of PMMA and PMMA-based nanocomposites was conducted using TGA analysis. The mass loss curves and corresponding derivative curves (DTG) are shown in Fig. (8). The temperatures where 5% degradation occurs ($T_{5\%}$), 10% degradation ($T_{10\%}$), mid-point degradation ($T_{50\%}$), maximum degradation rate (T_{max}), and residual mass (char) at 600°C are summarized in the Table (2). The $T_{5\%}$ for PMMA was 217°C, while the corresponding $T_{5\%}$ for the nanocomposites containing 1% and 3%, MMT-ADM_{18} was significantly increased to 256 and 279°C respectively. Increasing the MMT-ADM_{18} amount from 1 to 3% increased $T_{50\%}$ to 382 and 396°C, respectively, compared to pure

PMMA (370°C). Increasing MMT-ADM_{18} loading in the PMMA matrix results in an increase in $T_{5\%}$ by 39–62 °C, $T_{10\%}$ by 30–36 °C, and $T_{50\%}$ by 12–26 °C. A same trend was observed in the T_{max} values. Also, the residual mass of all nanocomposites is in accordance with the amount of MMT-ADM_{18} loaded, as expected. From the DTG curves shown in Fig. 8(b), the neat PMMA shows two stages of thermal degradation behavior. The first stage observed from 180 to 350°C, which can be split into two steps: decomposition of weak head-to-head linkages (180–260°C) and destruction of unsaturated chain ends (resulting from termination by disproportionation) at about 350°C. The second stage proceeds from 350°C up to 440°C and is caused by the random destruction of the PMMA chains **(Nikolaidis *et al.*, 2018; Patra *et al.*, 2011)**. It is clear that as the amount of MMT-ADM_{18} increases, the first step is decreased while the second step is shifted to higher temperature, implying a desirable protection from degradation. It is clear that the thermal stability of the PMMA/MMT-ADM_{18} nanocomposites is improved compared to virgin PMMA, as expressed by shifting the degradation curve to higher temperatures. The origin of this increase in decomposition temperatures has been attributed to either the ability of nanometric silicate layers to obstruct volatile gas produced by thermal decomposition or the MMT layers resisting heat transfer to PMMA due to the formation of a 'protection layer' by the MMT. Also, the increase in thermal stability may also be a result of the restricted thermal motion of the PMMA in the gallery. In addition, the improvements in thermal stability of PMMA-based nanocomposites were not only dependent on MMT loading but also related to proper dispersion, degree of exfoliation, and the interaction between the MMT-ADM_{18} and PMMA matrix **(Nikolaidis *et al.*, 2018)**.

Table (2): Thermal analysis data of PMMA/MMT-ADM_{18} nanocomposites

Sample	$T_{D5\%}$	$T_{D10\%}$	$T_{D50\%}$	T_{Max}	Char (%)
Neat PMMA	217	274	370	393	0
PMMA–1% MMT-ADM_{18}	256	304	382	397	1.2
PMMA–3% MMT-ADM_{18}	279	310	396	٤05	3.4

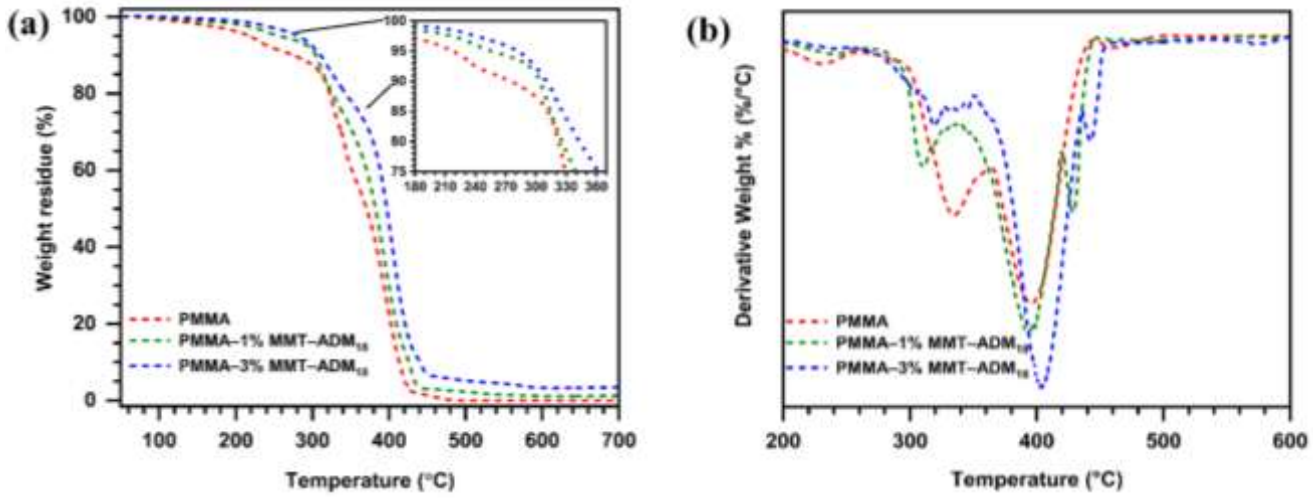

Fig. (8): (a) TGA and (b) DTG curves of PMMA and PMMA/MMT-ADM$_{18}$ nanocomposites with 1 and 3% MMT-ADM$_{18}$.

Conclusion

In this work, through a one-step miniemulsion polymerization process, modified MMT platelets were encapsulated within a PMMA core. During polymerization, for optimum compatibility with the monomer and to prevent platelet migration to the polymer/water interface, pre-modification of MMT was essential for successful encapsulation. The XRD data revealed that the MMT-ADM$_{18}$ was dispersed uniformly and exfoliated in the final latex. Additionally, TEM images demonstrated stable nanocomposite latexes comprised of MMT core and PMMA shell with diameters ranging from 320 to 450 nm were formed. The SEM image of the nanocomposite latexes also confirmed encapsulation, as MMT platelets were not observed on the nanocomposites surface. TGA results showed that all PMMA/MMT-ADM$_{18}$ nanocomposites showed substantial improvement in thermal stability as compared to a neat polymer; for example, $T_{D5\%}$, $T_{D10\%}$, and $T_{D50\%}$ were increased by 62°C, 36°C, and 26°C, respectively, with increasing amounts of MMT-ADM$_{18}$. Also, the T_{max} values showed the same trend.

References

Abulyazied, D.E.; and Ene, A., (2021). "An investigative study on the progress of nanoclay-reinforced polymers: Preparation, properties, and applications: A review." *Polymers*, 13: 4401-4419.

Abuzeid, M.A.; Bassuoni, M.T.; and Sakr, M.R., (2024). "Effect of Polymer/Nano-Clay Coatings on the Performance of Concrete with High-Content Supplementary Cementitious Materials under Harsh Exposures." *Materials*, 17: 1030.

Agag, T.; Akelah, A.; Abdelwahab, M.; Takeichi, T.; and Muto, H., (2010). "Vinylester resin-clay hybrids using

various intercalating agents." *J. Appl. Polym. Sci*, 115: 2060-2068.

Agag, T. and Takeichi, T., (2008). "Preparation and cure behavior of organoclay-modified allyl-functional benzoxazine resin and the properties of their nanocomposites." *Polym. Compos*, 29: 750-757.

Akelah, A.; Rehab, A.; Abdelwahab, M. and Betiha, M.A., (2017). "Synthesis and thermal properties of nanocomposites based on exfoliated organoclay polystyrene and poly(methylmethacrylate)." *Nanocomposites*, 3: 20-29.

Al-Muntaser, A.A.; Abdelghany, A.M., Abdelrazek, E.M.; Elshahawy, A.G., (2020). "Enhancement of optical and electrical properties of PVC/PMMA blend films doped with $Li_4Ti_5O_{12}$ nanoparticles." *J. Mater. Res. Technol*, 9: 789-797.

Al-Sabagh, A.M.; Betiha, M.A.; Osman, D.I., Hashim, A.I.; El-Sukkary, M.M., and Mahmoud, T., (2016). "A new covalent strategy for functionalized montmorillonite–poly(methyl methacrylate) for improving the flowability of crude oil." *RSC Adv*, 6: 109460-109472.

Álvarez-Bermúdez, O.; Adam-Cervera, I.; Landfester, K., and Muñoz-Espí, R., (2024). "Morphology Control of Polymer–Inorganic Hybrid Nanomaterials Prepared in Miniemulsion: From Solid Particles to Capsules." *Polymers*, 16: 2997.

Bai, C.; Ke, Y.; Hu, X.; Xing, L.; Zhao, Y.; Lu, S., and Lin, Y., (2020). "Preparation and properties of amphiphilic hydrophobically associative polymer/montmorillonite nanocomposites." *R. Soc. Open Sci*, 7: 200199.

Bakr, A.M.; Darwish, A.; Azab, A.A.; El Awady, M.E.; Hamed, A.A., and Elzwawy, A., (2024). "Structural, dielectric, and antimicrobial evaluation of PMMA/CeO_2 for optoelectronic devices." *Sci. Rep*, 14: 2548.

Bee, S.L.; Abdullah, M.A.A.; Bee, S.T.; Sin, L.T., and Rahmat, A.R., (2018). "Polymer nanocomposites based on silylated-montmorillonite: A review." *Prog. Polym. Sci*, 85: 57-82.

Cauvin, S.; Colver, P.J.; and Bon, S.A.F., (2005). "Pickering stabilized miniemulsion polymerization: preparation of clay armored latexes." *Macromolecules*, 38: 7887-7889.

Chencheni, A.; Belkhiri, S.; Tarchoun, A.F.; Abdelaziz, A.; Boucheffa, Y., and Trache, D., (2024). "Insights into the curing and thermal behavior of orthophtalic unsaturated polyester resin with organically modified montmorillonite nanoclay." *React. Kinet. Mech. Catal*, 1-23.

Dastjerdi, Z.; Cranston, E.D.; Berry, R.; Fraschini, C. and Dubé, M.A., (2019). "Polymer Nanocomposites for Emulsion-Based Coatings and Adhesives." *Macromol. React. Eng*, 13: 1800050-1800065.

Faucheu, J.; Gauthier, C.; Chazeau, L.; Cavaille, J.Y.; Mellon, V., and Lami, E.B., (2010). "Miniemulsion polymerization for synthesis of structured clay/polymer nanocomposites: short review and recent advances." *Polymer*, 51: 6-17.

Franco-Urquiza, E.A., (2021). "Clay-Based Polymer Nanocomposites: Essential Work of Fracture.", 13: 2399-2414.

Godiya, C.B.; Marcantoni, E.; Dunjić, B.; Tomić, M.; Nikolić, M.S.; Maletaškić, J. and Djonlagić, J., (2021). "Effect of

organoclay modifier structure on the viscoelastic and thermal properties of poly(methyl methacrylate)/organoclay nanocomposites." *Polym. Bull,* 78: 2911-2932.

Gul, S.; Kausar, A.; Muhammad, B. and Jabeen, S., (2016). "Research progress on properties and applications of polymer/clay nanocomposite." *Polym. Plast. Technol. Eng,* 55: 684-703.

Guo, F.; Aryana, S.; Han, Y., and Jiao ,Y., (2018). "A review of the Synthesis and Applications of Polymer-Nanoclay Composites." *Appl. Sci,* 8: 1696-1715.

Guo, Y.X.; Liu, J.H.; Gates, W.P., and Zhou, C.H., (2020). "Organo-modification of montmorillonite." *Clays Clay Miner,* 68: 601-622.

Idumah, C.I.; Okonkwo, U.C., and Obele, C.M., (2022). "Recently emerging advancements in montmorillonite polymeric nanoarchitectures and applications." *Clean. Mater,* 4: 100071-100107.

Jansen, T.G.T.; Meuldijk, J.; Lovell, P.A., and Van Herk, A.M., (2016). "On the miniemulsion polymerization of very hydrophobic monomers initiated by a completely water-insoluble initiator: thermodynamics, kinetics, and mechanism." *J. Polym. Sci., Part A:Polym. Chem,* 54: 2731-2745.

Kalendova, A.; Kupkova, J.; Urbaskova, M., and Merinska, D., (2024). "Applications of Clays in Nanocomposites and Ceramics." *Minerals,* 14: 93.

Lovell, P.A., and Schork, F.J., (2020). "Fundamentals of emulsion polymerization." *Biomacromolecules,* 21: 4396-4441.

Mang, J., and Han, M., (2010). "Mechanical Properties of IIR/OMMT Nanocomposites via Melt-Compounding and Solution Process." *J. Nanosci. Nanotechnol,* 10: 211-216.

Moraes, R.P.; Valera, T.S.; Demarquette, N.R.; Oliveira, P.C.; Da Silva, M.L.C.P., and Santos, A.M., (2009). "Influence of granulometry and organic treatment of a Brazilian montmorillonite on the properties of poly(styrene- co- n- butyl acrylate)/layered silicate nanocomposites prepared by miniemulsion polymerization." *J. Appl. Polym. Sci,* 112: 1949-1958.

Muñoz-Espí, R.; Weiss, C.K., and Landfester, K., (2012). "Inorganic nanoparticles prepared in miniemulsion." *Curr. Opin. Colloid Interface Sci,* 17: 212-224.

Murugesan, S.; and Scheibel, T., (2020). "Copolymer/Clay Nanocomposites for Biomedical Applications." *Adv. Funct. Mater,* 30: 1908101-1908127.

Nikolaidis, A.K., and Achilias, D.S., (2018). "Thermal degradation kinetics and viscoelastic behavior of poly(methyl methacrylate)/organomodified montmorillonite nanocomposites prepared via in situ bulk radical polymerization." *Polymers,* 10: 491.

Okamoto, M., (2023). "Polymer nanocomposites." *Eng,* 4: 457-479.

Patra, N., Salerno; M., Malerba, M.; Cozzoli, P D., and Athanassiou, A., (2011). "Improvement of thermal stability of poly(methyl methacrylate) by incorporation of colloidal TiO2 nanorods." *Polym. Degrad. Stab,* 96: 1377-1381.

Pieters, K., and Mekonnen, T., (2024). "Progress in waterborne polymer dispersions for coating applications:

commercialized systems and new trends." *RSC Sustain*.

Schork, F.J., (2024). "Monomer Equilibrium and Transport in Emulsion and Miniemulsion Polymerization." *Biomacromolecules*.

Silva, R.D.; Chaparro, T.D.C.; Monteirom I.S.; Dugas, P.Y.; D'agosto, F.; Lansalot, M.; Martins dos Santos, A., and Bourgeat-Lami, E., (2019). "Tailoring the morphology of polymer/montmorillonite hybrid latexes by surfactant-free emulsion polymerization mediated by amphipathic MacroRAFT agents." *Macromolecules,* 52: 4979-4988.

Terchi, S.; Hamrit, S.; Ladjal, N.; Bachari, K., and Ben Rhaiem, H., (2024). "Synthesize of exfoliated poly(methylmethacrylate)/organomontorillonite nanocomposites by in situ polymerization: structural study, thermal properties and application for removal of azo dye pollutant." *J. Therm. Anal. Calorim,* 149: 2161-2177.

Thickett, S.C., and Teo, G.H., (2019). "Recent advances in colloidal nanocomposite design via heterogeneous polymerization techniques." *Polym. Chem,* 10: 2906-2924.

Uddin, F., (2018). *Montmorillonite: An introduction to properties and utilization* Vol. 817): IntechOpen London, UK.

Uddin, M.N.; Hossain, M.T.; Mahmud, N.; Alam, S.; Jobaer, M.d.; Mahedi, S.I., and Ali, A., (2024). "Research and applications of nanoclays: A review." *SPE Polym,* 5: 507-535.

Voorn, D.J.; Ming, W., and Van Herk, A.M., (2006). "Polymer−clay nanocomposite latex particles by inverse pickering emulsion polymerization stabilized with hydrophobic montmorillonite platelets." *Macromolecules,* 39: 2137-2143.

Voorn, D.J.; Ming, W., and Van Herk, A.M., (2006). "Clay platelets encapsulated inside latex particles." *Macromolecules,* 39: 4654-4656.

Wang, H.; Wang, L.; Meng, S.; Lin, H.; Correll, M. and Tong, Z., (2020). "Nanocomposite of graphene oxide encapsulated in polymethylmethacrylate (PMMA): pre-modification, synthesis, and latex stability." *J. Compos. Sci,* 4: 118.

Youssef, A.M.; Malhat, F.M.; Hakim, A.A. and Dekany, I., (2017). "Synthesis and utilization of poly(methylmethacrylate) nanocomposites based on modified montmorillonite." *Arab. J. Chem,* 10: 631-642.

Yu, C.; Ke, Y.; Deng, Q.; Lu, S.; Ji, J.; Hu, X. and Zhao, Y., (2018). "Synthesis and Characterization of Polystyrene-Montmorillonite Nanocomposite Particles Using an Anionic-Surfactant-Modified Clay and Their Friction Performance." *Appl. Sci,* 8: 964-981.

Zengeni, E.; Hartmann, P.C. and Pasch, H., (2013). "Highly Filled Polystyrene/Laponite Hybrid Nanoparticles Prepared Using the Ad-miniemulsion Polymerisation Technique." *Macromol. Chem. Phys,* 214: 62-75.

Zhu, T.T.; Zhou, C.H.; Kabwe, F.B.; Wu, Q.Q.; Li, C.S. and Zhang, J.R., (2019). "Exfoliation of montmorillonite and related properties of clay/polymer nanocomposites." *Appl. Clay Sci,* 169: 48-66.

Zidan, T.A., (2020). "Synthesis and characterization of modified properties of poly(methyl methacrylate)/organoclay nanocomposites." *Polym. Compos,* 41: 564-572.

تغليف صفائح المونتموريلونيت العضوية من خلال بلمرة المستحلب المصغر داخل جزيئات اللاتكس المصنوعة من مادة البولي (ميثيل ميثاكريلات): التحضير والخصائص الحرارية

أحمد عكيلة ، أحمد رحاب ، هشام حرحش ، حماده مندور*

قسم الكيمياء- كلية العلوم- جامعة طنطا

في هذه الدراسة ، تم بنجاح تغليف المونتموريلونيت (MMT) في بولي (ميثيل ميثاكريلات) (PMMA) عن طريق بلمرة المستحلب المصغر. أولا، تم استخدام (*N*-allyl-*N*,*N*-dimethyloctadecan-1-aminium bromide (ADM_{18}) ،وهي مادة خافضة للتوتر السطحي قابلة للبلمرة لتعديل المونتموريلونيت عبر التبادل الأيوني لكي يتوافق مع المونومر وكذلك لتكوين رابطة تساهمية مع البوليمر. بعد ذلك ، تم دمج الطفلة المعدلة في ميثيل ميثاكريلات، جنبا إلى جنب مع خافض للتوتر السطحي، ومثبت، وبادئ، للحصول على مستحلب نانومتري مستقرعن طريق بلمرة المستحلب المصغر. تم استخدام FTIR وXRD وSEM وTEM وTGA للتحقق من صحة المتراكبات وتوصيف الخصائص الحرارية للمتراكبات النانومترية الناتجة. أشار FTIR إلى حدوث تفاعل بين مجموعة الهيدروكسيل الهيكلية للمونتموريلونيت وجزء الكربونيل الخاص بالبوليمر. أظهرت XRD أن شكل المتركبات النانومترية قد تقشر. أظهرت صور TEM أن متراكبات نانومترية مستقرة تتكون من نواة من المونتموريلونيت ومحاطة بغلاف من البوليمر (PMMA) بأقطار تتراوح من ٣٢٠ إلى ٤٥٠ نانومتر قد تشكلت. أظهرت نتائج TGA تحسنا كبيرا في الاستقرار الحراري للمتراكبات النانومترية.